ENGINEERING MATERIALS

COMMUNICATION

DOI: 10.1002/adem.201600048

Deterministic Switching of Hierarchy during Wrinkling in Quasi-Planar Bilayers**

By *Sourabh K. Saha*[*,1] and *Martin L. Culpepper*

The lack of affordable and scalable manufacturing processes for pattern generation is a bottleneck in transitioning several promising nano-enabled technologies from research laboratories to real-world adoption.[1] In contrast to the existing slow and expensive pattern generation techniques, self-organization-based processes provide an alternate route to scale-up by enabling low-cost patterning over large areas.[2–4] For example, uniform 1-D periodic wrinkled patterns can be generated over large areas via uniaxial compression of flat bilayers.[5,6] Such patterns have been used in the past to fabricate tunable nanofluidic channels,[7–8] tunable diffraction gratings,[9,10] and for low-cost nanometrology.[11,12] Although pattern fabrication via wrinkling is scalable, this process is currently of limited practical import. This is primarily because predictive design of wrinkled patterns is limited to a small set of elementary geometric patterns,[13–16] that is, it is not possible to deterministically predict complex multi-period wrinkled patterns for a given set of process parameters. This makes it difficult to fabricate the desired wrinkled patterns with any certainty. We have overcome this limitation for the specific case of hierarchical wrinkled patterns by demonstrating deterministic switching of hierarchy during compression of quasi-planar bilayers.

In the past, several empirical studies have demonstrated the feasibility of hierarchical wrinkle formation by "adding up" patterns.[17–21] Physical pattern addition is often achieved by compressing a pre-patterned non-flat bilayer.[19–21] This non-flat geometry can be conveniently generated via recursive wrinkling, that is, by replicating/imprinting wrinkled patterns that are fabricated via compression of flat bilayers.[19] As wrinkled patterns form due to non-linear buckling bifurcation phenomena, the observed composite patterns are not equivalent to a linear superposition of the elementary patterns. To predict these composite patterns, approximate semi-empirical models may be generated by reducing the pre-patterned system to either a flat bilayer[21] or a curved bilayer with a non-zero average global curvature.[22] Unfortunately, such approximations do not capture the physical effect of quasi-planar geometry on pattern formation.

A quasi-planar geometry is fundamentally distinct in form and behavior from both flat and curved geometry and refers to an "almost" flat surface geometry that has periodic spatial variations in the local curvature but a zero average global curvature. Herein, we investigate the effect of form of quasi-planar bilayers on the pattern formation behavior by identifying how the pre-pattern geometry fundamentally alters the deformation energy during compression of such systems. We show that the emergence of hierarchy during compression of quasi-planar bilayers is determined by two competing effects that arise due to the non-flat periodic geometry of such systems. As a result, emergence of hierarchy is preceded by a mode-locked state during which the quasi-planar form persists.

1. Results and Discussion

We have fabricated quasi-planar bilayer systems by generating glassy thin films on top of pre-patterned and stretched elastomeric base layers. Glassy thin films were generated by plasma oxidation of the polydimethylsiloxane (PDMS) base layers;[23,24] pre-patterns were generated in the base by replicating single-period wrinkled patterns onto the base during curing. The pre-patterns were aligned such that the directions of periodicity and pre-stretch were collinear.[25,26] Upon gradual release of the stretch in the base, one

[*] *Dr. S. K. Saha, Prof. M. L. Culpepper*
Department of Mechanical Engineering, Massachusetts Institute of Technology, 77 Massachusetts Ave, Cambridge, Massachusetts 02139, USA
E-mail: sourabh@alum.mit.edu
[1] *Present address: Materials Engineering Division, Lawrence Livermore National Laboratory, 7000 East Avenue, PO Box 808, L-782, Livermore, California 94551, USA*

[**] *This work was partly performed under the auspices of the U.S. Department of Energy by Lawrence Livermore National Laboratory under contract DE-AC52-07NA27344. S.K.S. utilized the Postdoctoral funding for independent research available at LLNL to write this manuscript (#LLNL-JRNL-680043). We thank Elisabeth L. Shaw at CMSE, MIT for technical assistance with AFM imaging. Conflict of interest: Patent applications related to this work have been filed at the USPTO that are co-invented by S.K.S. and M.L.C. and assigned to S.K.S. (Supporting Information is available online from Wiley Online Library or from the author).*
The copyright line of this article was changed 2 June 2016 after initial publication.

observes a mode lock-in behavior wherein the amplitude of the pre-pattern increases while maintaining the single-period pre-pattern geometry. With further release of the stretch, a multi-period hierarchical mode emerges beyond a critical threshold. The patterns are reversible around this transition strain (ε_t), that is, the hierarchical mode can be switched back to the single-period pre-pattern mode by increasing the stretch in the base. This phenomenon is illustrated in Figure 1.

The mode lock-in behavior is a distinct characteristic of quasi-planar systems and can be tuned via process parameters. For example, when the initial stretch in the base layer is lower than the transition strain, no hierarchical wrinkles are observed upon full pre-stretch release. One such representative mode-locked pattern is depicted in Figure 1d. We have also verified this mode lock-in behavior via finite element simulations, as illustrated in Figure 1c. Simulations were performed by modeling the non-linear buckling bifurcation phenomenon that occurs during compression of pre-patterned bilayers. Custom codes were written to transform flat bilayers into quasi-planar bilayers by applying large mesh perturbations; these codes are available elsewhere.[27]

The mode lock-in behavior arises due to the competing effects of the period and the amplitude of pre-patterns on the deformation energy. In the absence of a pre-pattern, a flat bilayer system bifurcates into its natural period, that is, into the period that minimizes the deformation energy. By pre-patterning the base with a period that is different from the natural pattern, one "forces" the bilayer system into a higher energy deformation state. Concurrently, an energy advantage arises due to the non-flat geometry. This is because the deformation energy of a flat system is higher than that of a strain-free non-flat system when compressed by the same strain (see Supporting Information Section S4.2). Hierarchical wrinkles are formed due to a competition between these two effects: energy penalty due to non-natural period and energy advantage due to non-zero amplitude.

Mode lock-in at the onset of pre-stretch release occurs because the energy advantage due to non-zero amplitude dominates the energy penalty due to non-natural period. This energy advantage forces the system to stay locked into an otherwise energetically unfavorable mode. As strain affects amplitude and period differently, these energy penalties and advantages vary with the strain. With further pre-stretch release, the energy penalty gradually starts dominating. Hierarchical wrinkles emerge when this penalty exceeds the energy advantage. In finite element simulations and physical systems, this transition can be identified by the emergence of the natural period in the patterns. The Fast Fourier Transform of the simulated patterns shown in Figure 2 demonstrates how emergence of the natural period results in hierarchy. As illustrated in Figure 2d, this mode transition is accompanied with a distinct change in the slope of deformation energy versus strain plot. Herein, we have separately captured these two competing effects via

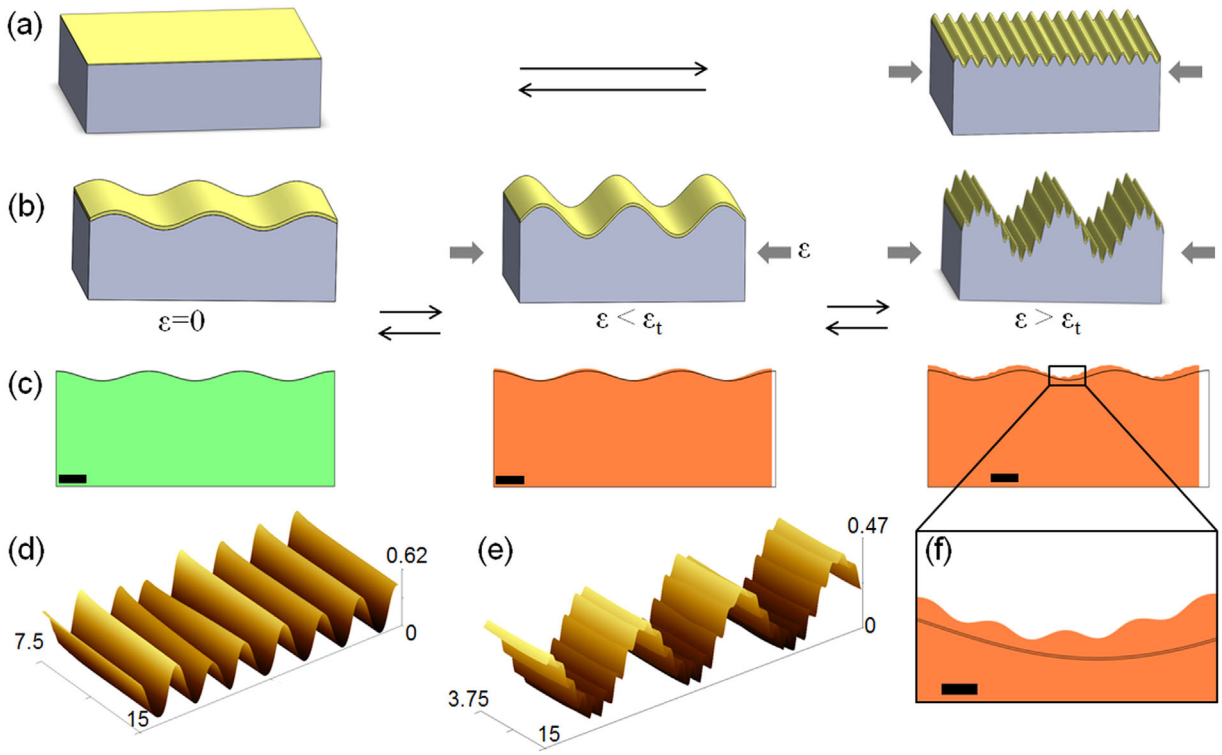

Fig. 1. Schematic representation of pattern formation during (a) compression of planar bilayers depicting formation of natural wrinkles and (b) compression of quasi-planar bilayers depicting mode lock-in at low strains and hierarchy at high strains. (c) Effect of compression on a quasi-planar bilayer as observed during finite element simulations. Scale bars are 1.5 μm long. The pre-pattern period, amplitude, intermediate strain, final strain, and natural period were (5 μm, 219 nm, 1.4%, 3.5%, 0.5 μm). (d) Atomic force microscope images of fabricated mode-locked and (e) hierarchical wrinkles. Length unit for scale is μm. Pre-pattern period, amplitude, strain, and natural period were (2.6 μm, 272 nm, 9.9%, 1.6 μm) for mode-locked and (4.6 μm, 110 nm, 6.6%, 0.8 μm) for hierarchical wrinkles. (f) Zoomed image of hierarchical pattern generated during finite element simulations. Scale bar is 250 nm long.

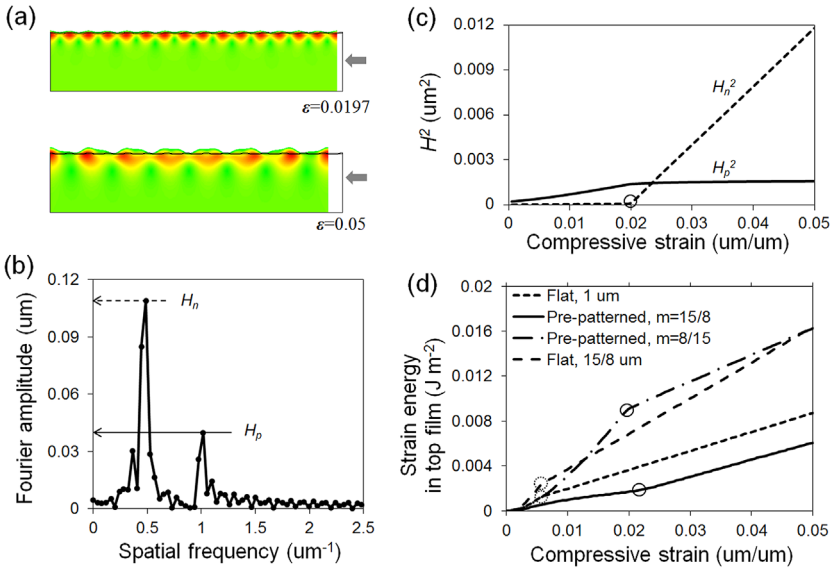

Fig. 2. (a) First principal strain in the mode-locked and the hierarchical states evaluated via finite element simulations. (b) Fourier-amplitude power spectrum of the height of the mid-plane of the top film at a strain of 5%. The pre-pattern period, amplitude, and natural period were (1 μm, 16 nm, 1.875 μm). (c) Evolution of the square Fourier-amplitude of the pre-pattern (solid line) and natural (dotted line) modes with strain. (d) Evolution of the strain energy in the top film with strain for the pre-patterned and the corresponding flat bilayers. Solid circles denote transition of pre-patterned bilayers into hierarchical mode whereas dotted circles denote transition of flat bilayers into natural mode. Amplitude of pre-patterns was 16 nm. In (c) and (d), the transition strains obtained from evolution of Fourier-amplitude and strain energy are identical (m = 8/15).

analytical models to predict the transition of quasi-planar bilayers into hierarchical modes.

To separately quantify the "energy advantage" due to non-zero amplitude, we consider the special case wherein the period of pre-patterns (λ_p) is equal to the natural period (λ_n). Such quasi-planar systems do not demonstrate hierarchy because there is no competing energy penalty. We have modified the linear elastic model proposed by Groenewold[13] to model the effect of non-zero pre-pattern amplitude (A_p) on the scaled strain energy as (details in Supporting Information Section S4.2):

$$\frac{U_{p,n}}{U_{f,n}} = 1 - 2n^2\left[\left(1+(1/n)^2\right)^{0.5} - 1\right] \qquad (1)$$

This scaled strain energy is a ratio of the strain energy in a system that is pre-patterned with the natural period ($U_{p,n}$) and in an equivalent flat system ($U_{f,n}$). This ratio varies between one and zero; a value of one corresponds to a pre-pattern with zero amplitude, that is, a flat system. Thus, a low value for this ratio corresponds to a high "energy advantage." Here, "n" is the ratio of amplitudes of the pre-pattern and the natural pattern, that is, $n = A_p/A_n$. As illustrated in Figure 3a, "energy advantage" in the system decreases with an increase in the compressive strain. The initial deviation of the computed "energy advantage" from the predicted values is due to the presence of the longitudinal film compressive mode in flat bilayers before the onset of wrinkling. In pre-patterned bilayers, this longitudinal compression is negligibly small (see Supporting Information Section S4.2) and does not affect pattern formation.

As the natural pattern is physically observable, the natural period (λ_n) and amplitude (A_n) may be empirically determined by observing the period and amplitude of wrinkles formed in an equivalent flat bilayer system. Within these geometric parameters, the effect of thin film thickness (h) and ratio of Young's moduli (η) is incorporated in the natural period ($\lambda_n \sim h \cdot \eta^{1/3}$) whereas the effect of strain (ε) is incorporated in the amplitude of the natural mode ($A_n \sim \lambda_n \cdot \varepsilon^{0.5}$).

The energy penalty due to non-natural pre-pattern can be quantified by evaluating the strain energy of a hypothetical system that bifurcates into the pre-pattern period from a flat state. When a flat bilayer system deforms to form wrinkles of period λ_p, the scaled strain energy is as follows:

$$\frac{U_{f,p}}{U_{f,n}} = \frac{1+2m^3}{3m^2} \qquad (2)$$

Here, $U_{f,p}$ is the strain energy in the flat bilayer if it bifurcates into wrinkles of same period as the pre-pattern and "m" is the ratio of period of pre-pattern to natural period, that is, $m = \lambda_p/\lambda_n$. The energy penalty increases as the pre-pattern period deviates away from the natural period. As illustrated in Figure 3b, the penalty demonstrates a distinct asymmetry about the natural period, that is, the increase in penalty is steeper for periods that are lower than the natural period. Asymmetric behavior arises due to the difference in the source

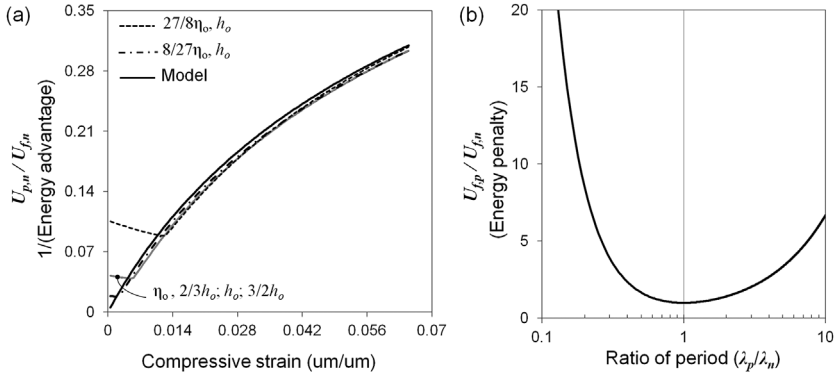

Fig. 3. Effect of pre-pattern geometry on strain energy. (a) Computationally evaluated energy advantage for the special case when the pre-pattern and natural periods are identical. Energy advantage was evaluated as the reciprocal of the ratio of the strain energy in the top film of the pre-patterned and flat bilayers. The film thickness h_o was 75 nm, Young's moduli ratio η_o was 1190.5, and the pre-pattern amplitude was 5% of the period. (b) Analytically evaluated energy penalty in wrinkled bilayers for the special case when the pre-pattern amplitude is zero.

ADVANCED ENGINEERING MATERIALS

of penalty; penalty for higher periods arises due to the base whereas penalty for lower periods arises due to the thin film. This is because strain energy in the base is directly proportional to the period whereas strain energy in the film is inversely proportional to the square of the period.[13] For periods higher than the natural period, penalty arises due to an increase in the energy of the base; whereas for periods lower than the natural period, penalty arises due to an increase in the energy of the film. Asymmetry arises because the scaling of strain energy with period is linear for the base but quadratic for the film. As discussed later, this asymmetry is also reflected in the transition behavior and serves as a qualitative internal consistency test to verify the analytical model.

When a non-natural pre-patterned quasi-planar surface is compressed, the energy advantage and the energy penalty co-exist. The scaled deformation energy of a quasi-planar bilayer system during compression is given by the following (details in Supporting Information Section S4.4):

$$\frac{U_{p,p}}{U_{f,n}} = \frac{1+2m^3}{3m^2}\left[1-2(n/m)^2\left(\left(1+(m/n)^2\right)^{0.5}-1\right)\right] \quad (3)$$

Here, $U_{p,p}$ is the strain energy in the quasi-planar bilayer that is pre-patterned with a period that is different from the natural period. At the onset of pre-stretch release, this ratio of energy is less than one thereby indicating that the pre-patterned mode is energetically favorable over the natural mode. The transition to hierarchy from mode-locked state occurs when this energy ratio exceeds one. Beyond the transition strain, the growth of the pre-patterned mode is energetically unfavorable with respect to the growth of the hierarchical mode that comprises the pre-patterned and natural modes. The transition criterion captured by Equation 3 may be represented entirely in terms of the geometrical parameters "n" and "m" as follows:

$$n_c = \frac{\left|1+2m^3-3m^2\right|}{\sqrt{12(1+2m^3)}} \quad (4)$$

At the onset of compression, the amplitude ratio "n" is infinitely large because the amplitude of the natural period is zero. With increasing compressive strain, the natural amplitude of the hypothetical equivalent flat bilayer increases along with a decrease in the amplitude ratio "n." As long as the amplitude ratio remains higher than the critical amplitude ratio "n_c," only the single-period pre-pattern exists. Physically, this manifests as an increase in the amplitude of the mode-locked state with an increase in the strain. Upon further compression, hierarchical patterns emerge when the amplitude ratio "n" falls below the critical amplitude ratio "n_c." Using kinematic relationships, the corresponding transition strain (ε_t) is evaluated as follows:

$$\varepsilon_t = \left[\pi\left(A_p/\lambda_p\right)(m/n_c)\right]^2 \quad (5)$$

As the geometric parameters that govern this transition are physically observable, one can accurately predict the transition behavior even with limited system knowledge about materials or applied strain. The universal phase diagram that represents this lock-in/hierarchy transition is shown in Figure 4. This phase diagram is applicable to all feasible combinations of process parameters and provides a powerful predictive tool to deterministically switch hierarchy in a variety of quasi-planar bilayers.

We have verified the accuracy of the phase diagram by comparing the analytical model against empirical data and finite element simulations. During experiments, wrinkled surfaces were imaged upon full pre-stretch release with an atomic force microscope to identify the state of the pattern as being either mode locked or hierarchical. During simulations, the critical amplitude ratio for transition was evaluated by measuring the transition strain for a set of pre-determined period ratio and pre-pattern amplitude. As illustrated in Figure 4, finite element simulations and experiments collectively confirm the accuracy of the analytical phase diagram. Additionally, an internal consistency check was performed to verify that the asymmetry in the energy penalty is accurately reflected in the asymmetry of the phase diagram. As non-natural periods with a period ratio less than unity have a steeper energy penalty, they force the quasi-planar systems to stay longer in the mode-locked state. This is reflected in the phase diagram in the form of a larger mode-locked region for period ratios less than unity.

The phase diagram presented here enables one to make rational design decisions that cannot be made via prevalent empirical techniques that rely on trial-and-error. For example, when tunable wrinkles are desired one may select the pre-pattern and natural patterns with either $m>1$ or $m<1$. Although similar hierarchical wrinkles can be theoretically obtained for both of these cases, based on the phase diagram we now know that the first combination provides a larger

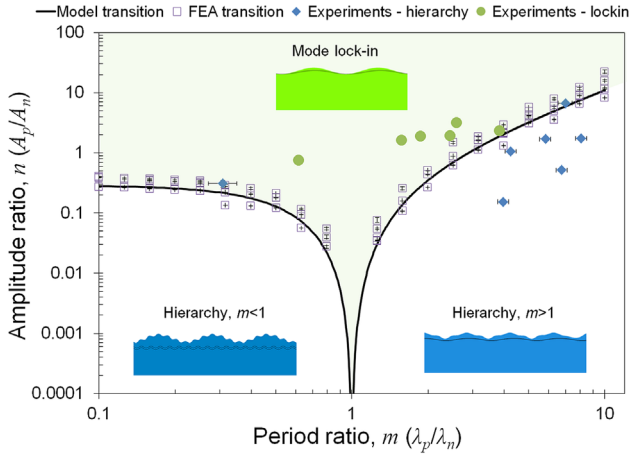

Fig. 4. Phase diagram for transition of pre-patterned surfaces from the mode locked into the hierarchical state. Experimental data represent the final state of the wrinkles (Supporting Information Table S3). Finite element simulations represent the transition criterion. Pre-pattern amplitude was varied within 0.13–45.25% of natural period (Supporting Information Table S4), natural period was 2.5 μm, the film thickness was varied in the range of (0.5–2) times 50 nm and the Young's moduli ratio was varied in the range of (0.125–8) times 1190.5.

accessible design-space for hierarchy whereas the second combination favors mode lock-in. One can also deduce from the phase diagram and Equation 5 that tunability of hierarchy is lost when the pre-pattern period is substantially higher than the natural period, that is, higher by a factor of at least 10. For such systems, the transition strain is negligibly small and one would fail to observe mode lock-in as a distinct state; instead, hierarchical wrinkles would seem to emerge immediately at the onset of pre-stretch release. We suspect that this is one of the reasons why the mode lock-in phenomenon has not been reported in the past within the context of wrinkling of pre-patterned surfaces.

2. Conclusions

Herein, we have generated the process knowledge that enables one to perform predictive design and fabrication of tunable hierarchical structures for the special case of single-period quasi-planar bilayers. Such tunable structures find applications in tunable gratings, microfluidics, and control of adhesion and wetting properties.[28,29] Specifically, hierarchical wrinkles with a period ratio of 1–2 can be used as shape-tunable optical gratings wherein the shape can be tuned via strain; whereas, hierarchical wrinkles with a period ratio of 5–10 may be used as tunable microfluidic channels wherein the lower period wrinkles generate tunable roughness on the surface of the larger period channels. Use of multi-period quasi-planar surfaces would broaden the applications of hierarchical wrinkles beyond these specific cases. By identifying the fundamental link between geometric form and pattern formation behavior of single-period quasi-planar geometries, we provide the framework that is required to understand pattern formation in more complex multi-period quasi-planar geometries.

3. Experimental

3.1. Curing of PDMS Films

Flat PDMS base films were fabricated by casting and thermally curing a two-part polydimethylsiloxane (PDMS) silicone elastomer mix that is commercially available from Dow Corning (Sylgard 184). The two parts were mixed by combining 12 parts of resin and one part of curing agent by weight. After degassing the mixture, curing was performed via a two-step thermal curing process so as to minimize the volumetric shrinkage in the film. Alignment features were generated on the bottom surface of the films by casting and curing the mixture in custom-made aluminum molds. These alignment features were later used to align the direction of stretch with the wrinkle pre-patterns.

3.2. Fabrication of Pre-Stretched Bilayers and Wrinkles

The cured PDMS films were manually cut into individual coupons that were approximately 20 mm wide, 1.9–2.2 mm thick, and had a clamped length of 37.5 mm. These coupons were then mounted and stretched on a custom-made precision tensile stage.[25] The accuracy of the clamped length was ensured by mating the alignment features on the coupons to the corresponding features on the stage. The entire stage with the stretched coupon was then inserted into a vacuum chamber and exposed to low-pressure RF air plasma. The air plasma chemically modifies the surface and generates a glassy thin film on top of the PDMS layer that has a Young's modulus of 3.2 ± 0.78 GPa[26] and is 10–100 nm thick. The thickness of the glassy film can be tuned by controlling the duration of the plasma exposure. The plasma oxidation process was calibrated to link the observed period to the duration of exposure; the calibration chart is available in the Supporting Information. After plasma oxidation, wrinkles were generated by gradually releasing the stretch in the base layer thereby causing the top glassy layer to compress and buckle.

3.3. Fabrication of Quasi-Planar Base Layers

Quasi-planar base layers were fabricated by imprinting wrinkled surfaces onto the base during the thermal curing process. Imprinting was performed by gradually and "gently" placing the coupons with the wrinkled surfaces on top of the curing material after the onset of curing but before gelation. Alignment of the pre-patterns to the subsequent direction of stretch was achieved by visually sensing and then aligning the alignment marks on the coupons with the alignment marks on the mold. It was observed that when imprinting is performed immediately at the beginning of curing, the coupons quickly sink to the bottom of the mold leading to an extremely thin and unusable quasi-planar base. Therefore, imprinting was delayed by several minutes after the onset of curing to ensure that the base film is sufficiently viscous to support the weight of the coupon. The protocol for imprinting is summarized in the Supporting Information and described in detail elsewhere.[26]

3.4. Metrology Protocol

The experimental data illustrated in Figure 4 were obtained by recording a scan of the wrinkled surface on an Atomic Force Microscope (AFM) when the pre-stretch in the pre-patterned base was fully released. The compressive strain in the top film was measured from the wrinkled profile by evaluating the total length of the curved profile. The pre-pattern amplitude and period and the natural period were directly measured for one set of experiments and indirectly via calibration of the plasma oxidation process for the other set. The observable geometric parameters of the experiments and details of the metrology protocol are available in the Supporting Information. Uncertainty in the experimental data arises due to spatial variation in the measurement of the pre-pattern and the calibration curves. This uncertainty has been previously characterized elsewhere in detail.[25] The error bars in Figure 4 are based on this characterization and quantify the standard deviation in the period and amplitude of $\pm 5\%$ for direct measurements and $\pm 6.5\%$ for indirect measurements.

3.5. Finite Element Simulations

Finite element modeling was performed by developing 2-D models of wrinkling using the Structural Mechanics module of the COMSOL 4.2 software package. These models were developed by implementing buckling of wide plates under the plane strain condition wherein the top film is a linear elastic material and the bottom layer is a Neo-Hookean material. A non-linear strain–displacement relationship was used for both layers to account for large angles during wrinkling. The bilayer was uniaxially compressed by simultaneously compressing the top and bottom layers. Modeling of wrinkle formation in flat bilayers was performed in two steps:[30] i) linear pre-buckling analysis to predict the mode shapes required for generating the perturbed mesh and ii) a non-linear post-buckling analysis on the perturbed mesh to predict the shape and amplitude of the wrinkles after

buckling bifurcation. Modeling of wrinkle formation in pre-patterned bilayers was performed on the perturbed mesh via a single-step nonlinear analysis. The perturbed mesh was generated from the pre-pattern geometry, as discussed in the Supporting Information. It was observed that additional mesh perturbations were not necessary to generate wrinkles during compression of pre-patterned bilayers. The transition strain (ε_t) at which the pre-patterned surfaces transition into the hierarchical mode was evaluated as the strain at which the absolute value of the second derivative of film energy versus strain has a peak. This criterion captures the change in the deformation mode that accompanies the transition from single-period mode-locked state to a two-period hierarchical state.

Article first published online: January 01, 2016
Manuscript Revised: April 12, 2016
Manuscript Received: January 26, 2016

[1] M. C. Roco, C. A. Mirkin, M. C. Hersam, *Nanotechnology Research Directions for Societal Needs in 2020: Retrospective and Outlook*, Springer Science & Business Media, Dordrecht, Netherlands **2011**, 1.
[2] I. Bita, J. K. W. Yang, Y. S. Jung, C. A. Ross, E. L. Thomas, K. K. Berggren, *Science* **2008**, *321*, 939.
[3] N. Bowden, S. Brittain, A. G. Evans, J. W. Hutchinson, G. M. Whitesides, *Nature* **1998**, *393*, 146.
[4] S. Y. Chou, L. Zhuang, *J. Vac. Sci. Technol. B* **1999**, *17*, 3197.
[5] Y. Mei, S. Kiravittaya, S. Harazim, O. G. Schmidt, *Mater. Sci. Eng. R: Rep*. **2010**, *70*, 209.
[6] J. Genzer, J. Groenewold, *Soft Matter* **2006**, *2*, 310.
[7] S. Chung, J. H. Lee, M.-W. Moon, J. Han, R. D. Kamm, *Adv. Mater.* **2008**, *20*, 3011.
[8] D. Huh, K. L. Mills, X. Zhu, M. A. Burns, M. D. Thouless, S. Takayama, *Nat. Mater.* **2007**, *6*, 424.
[9] C. Yu, K. O'Brien, Y.-H. Zhang, H. Yu, H. Jiang, *Appl. Phys. Lett*. **2010**, *96*, 041111.
[10] C. Harrison, C. M. Stafford, W. Zhang, A. Karim, *Appl. Phys. Lett*. **2004**, *85*, 4016.
[11] J. Y. Chung, J.-H. Lee, K. L. Beers, C. M. Stafford, *Nano Lett*. **2011**, *11*, 3361.
[12] C. M. Stafford, S. Guo, C. Harrison, M. Y. M. Chiang, *Rev. Sci. Instrum*. **2005**, *76*, 062207.
[13] J. Groenewold, *Phys. A* **2001**, *298*, 32.
[14] H. Jiang, D.-Y. Khang, J. Song, Y. Sun, Y. Huang, J. A. Rogers, *Proc. Natl. Acad. Sci*. **2007**, *104*, 15607.
[15] S. Cai, D. Breid, A. J. Crosby, Z. Suo, J. W. Hutchinson, *J. Mech. Phys. Solids* **2011**, *59*, 1094.
[16] J. W. Hutchinson, *Philos. Trans. R. Soc. A: Math. Phys. Eng. Sci*. **2013**, *371*, 20120422.
[17] K. Efimenko, M. Rackaitis, E. Manias, A. Vaziri, L. Mahadevan, J. Genzer, *Nat. Mater.* **2005**, *4*, 293.
[18] J. Yin, C. Lu, *Soft Matter* **2012**, *8*, 2528.
[19] A. Chiche, C. M. Stafford, J. T. Cabral, *Soft Matter* **2008**, *4*, 2360.
[20] C.-M. Chen, J. C. Reed, S. Yang, *Soft Matter* **2013**, *9*, 11007.
[21] J.-H. Lee, H. W. Ro, R. Huang, P. Lemaillet, T. A. Germer, C. L. Soles, C. M. Stafford, *Nano Lett*. **2012**, *12*, 5995.
[22] D. Breid, A. J. Crosby, *Soft Matter* **2013**, *9*, 3624.
[23] N. Bowden, W. T. S. Huck, K. E. Paul, G. M. Whitesides, *Appl. Phys. Lett*. **1999**, *75*, 2557.
[24] P. C. Lin, S. Yang, *Appl. Phys. Lett*. **2007**, *90*, 241903.
[25] S. K. Saha, M. L. Culpepper, *J. Micro Nano-Manuf*. **2015**, *3*, 041004.
[26] S. K. Saha, Ph.D. thesis, Massachusetts Institute of Technology, Cambridge, MA **2014**. http://hdl.handle.net/1721.1/93860
[27] S. K. Saha, M. L. Culpepper, MeshPerturb: MATLAB codes for mesh perturbation and automated pre and post processing of post-bifurcation analyses via COMSOL, **2014**. http://hdl.handle.net/1721.1/86934
[28] Z. Zhang, T. Zhang, Y. W. Zhang, K.-S. Kim, H. Gao, *Langmuir* **2011**, *28*, 2753.
[29] P.-C. Lin, S. Yang, *Soft Matter* **2009**, *5*, 1011.
[30] Y. Cao, J. W. Hutchinson, *J. Appl. Mech*. **2012**, *79*, 031019.

